Physicochemical, Vibrational and EPR Spectral Analysis of Soot-Filled Polystyrene

Abdusalom Umarov[1,2], Dilnavoz Kamalova[3], Nazokat Erdonova[2] and Nuriddin Valixanov[1]
[1]*University of Tashkent for Applied Sciences, Gavhar Str. 1, 100149 Tashkent, Uzbekistan*
[2]*Tashkent State Transport University, Universitetskaya Str. 2, 100095 Tashkent, Uzbekistan*
[3]*Navoi State Pedagogical Institute, Mustakillik Str. 3, 210100 Navoi, Uzbekistan*
rector@utas.uz , kamolatafu@utas.uz , abdusalom@inbox.ru, nuriddinvalikhanov@gmail.com

Keywords: Polystyrene, Soot, Composites, Physicochemical properties, EPR Spectra, Paramagnetic Centers, Chemical Bonds, Structural Features, X-Ray Fluorescence, Conductivity, Dielectric Losses, Frequency Dependence.

Abstract: In this work, we investigate patterns of these materials and their composites with an emphasis on vibrational spectroscopy and electron paramagnetic resonance (EPR) response. Such soot in the polystyrene matrix leads to structural and electronic changes that are attractive for advanced material uses. Vibrational spectra, served as an atomic level probe to the molecular interactions in these composites, displaying small shifts in the absorption bands; characteristic of soot modification in the polymeric matrix. EPR spectroscopy supported the evidence of stable paramagnetic centers in the soot-filled polystyrene composites. These centres were found to be responsible for the broadening of the EPR signal, suggesting possible magnetic-like behavior that may compete with classical magnetic materials. Elemental composition and bonding at the interface were also found to be composed of carbon, hydrogen, and oxygen by X-ray fluorescence analysis. Notably, the findings highlight that there is not a simple linear correspondence between soot content and the observed paramagnetic parameters implying that the interaction of soot distribution, interface bonding and defect types are more complex. These results provide new clues for the design of functional composites. In conclusion, the results contribute to our knowledge on the influence of carbonaceous fillers, such as soot, on polymer matrices. Possible applications are in advanced composites for electronics, sensing and magnetic materials, which could take advantage of novel structural and paramagnetic properties of soot-filled polymers. The present work provides insight into the multifunctional behavior of polymer−carbon composites and the necessity to study vibrational and EPR spectra together.

1 INTRODUCTION

Studies of soot particles dissolved in an aqueous medium, using an electron microscope, show that the size of the soot particles ranges from 25 to 35 nm. The soot particles have a spherical shape and consist of individual crystallites arranged in a disordered manner, with each crystallite comprising several parallel, flat lattices of carbon atoms [1].

Research on the dispersity of soot particles shows that their size distribution ranges from 10 to 100 nm, with a specific surface area of 250 m^2/g. Larger soot particles, with a diameter of about 300 μm, have been observed, and their specific surface area is 15 m^2/g, while the bulk density of soot is 100–350 kg/m^3.

As a result of electron microscope studies of soot, it has been established that it consists of particles ranging in size from 900 to 6000 nm, forming more or less branched chains, known as soot structures (Fig. 1).

Figure 1: Soot particles under an electron microscope.

In our studies, the infrared (IR) spectrum of PS is discussed in detail in the range from 3500 cm^{-1} to 70 cm^{-1}, where the vibrations of the benzene ring and the vibrations of the aliphatic hydrocarbon chain are considered independently of each other, and the validity of this approach is confirmed by the results of studies on partially deuterated samples [2]-[5].

In our experiments, both pure PS and composites based on it were obtained as follows: first, the PS was dissolved, and only then were these films pressed at the melting temperature. The results of the IR spectra (from 4000 cm^{-1} to 40 cm^{-1}) of KPM based on PS.7.1.S-0.01 and PS.7.1.S-0.02 are shown in Figures 2-3.

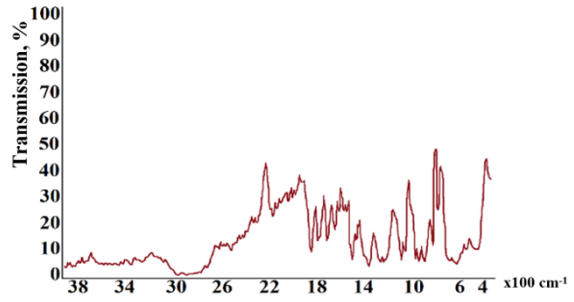

Figure 2: IR spectrum of PS.7.1.S-0.01.

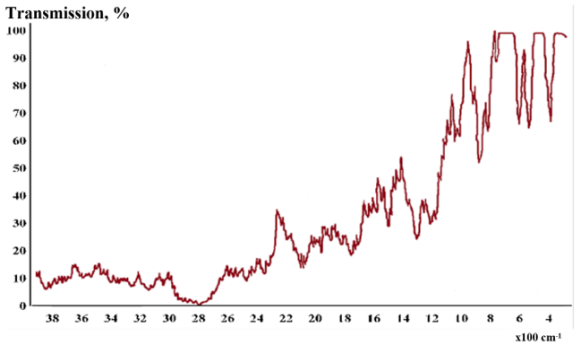

Figure 3: IR spectrum of PS.7.1.S-0.02.

It was established that at the initial stage of oxidation, a band appears in the spectrum at 1685 cm^{-1}, which was attributed to aromatic end groups. Only at a later stage does a weak band appear at 1720 cm^{-1}, caused by the absorption of aromatic aldehyde groups. Therefore, we suggest that 1774.6 cm^{-1} and 1713 cm^{-1} can be attributed to the stretching vibrations of C=O. Oxidation may occur during the technological process. When soot is added to PS, changes occur in the IR spectra (Fig. 2-3).

The first change is associated with the shift of most bands toward the short-wavelength region and a decrease in their intensity. The following vibrations were analyzed in detail: related to stretching (symmetric transformed into asymmetric), benzene ring, overtone fan, deformation, torsional, and others.

By comparing the IR spectra of PS.7.1 with a soot content of V1=0.02 and V1=0.01, significant changes are observed. The absorption band at 3629 cm^{-1} may represent O-H stretching vibrations, while the absorption bands at 3480 cm^{-1} and 3333 cm^{-1} may represent both O-H and C=O group stretching vibrations.

The ESR spectra of PS.7.1 with soot content V1=0.01 and V1=0.09 are shown in Figures 4-5, respectively [5]-[10].

The repeatability of the measurement results is quite high, and therefore, the radicals responsible for these signals can be considered stable. However, it is easy to notice that in all cases we are dealing with a scientific phenomenon – the strongest broadening of the ESR signal line, because the reality is that the soot of grade BS-100 itself gives a singlet signal (in air) with, and polystyrene does not signal at all, meaning it is diamagnetic [10]-[15]. In this case, it is reasonable to find an answer to the question – is the broadening related to the overlap of signals from various spin localization centers of different origins, or does it occur due to hyperfine splitting of electrons localized at paramagnetic centers of organic origin.

2 MANUSCRIPT PREPARATION

When PS is filled with carbon black V_1=0.01, changes occur in the IR spectra. The first change is associated with a shift of most bands to the short-wave region and a decrease in their intensity. Thus, the IR stretching vibration now appears at 3053 cm^{-1} (3040 cm^{-1} for PS). The symmetrical stretching vibration of CH_2 for pure PS is transformed into an antisymmetric stretching vibration of CH_2. The vibration of the benzene ring shifts from 1918 cm^{-1} (PS) to 1328 cm^{-1} (PS-C (0.01)). The doubled fan vibration of CH_2=CH appears at 1863 cm^{-1} (1846 cm^{-1} for PS). The stretching vibration of C=O shifts from 1774.5 cm^{-1} to 1734 cm^{-1}. However, this band is also characteristic of ^{12}CH. The second band of the C=O stretching vibration shifts from 1713.3 cm^{-1} to 1730 cm^{-1}. The latter is typical of $^{12}C^{16}O$ and is also close to =1725 cm^{-1} of diacetyl $(CH_3CO_2)_2$. The C=C stretching vibration in the CH_2=CH group shifts from 1646.6 cm^{-1} (PS) to 1650 cm^{-1}. The C=C vibration of the benzene ring 1568 cm^{-1} PS shifts to

1577 cm^{-1}. The CH_2 deformation vibration 1462.6 cm^{-1} shifts to 1473 cm^{-1}. It can also characterize =1473 cm^{-1} trimethylene oxide $(CH_2)_3O$. The second CH_2 bending vibration at 1420 cm^{-1} for PS shifts to 1434 cm^{-1} and it is interesting that diacetyl has =1444 cm^{-1}. The CH_2 fan vibration at 1348 cm^{-1} in PS-C(0.01) does not change. The second CH_2 fan vibration changes from 1305 cm^{-1} (PS) to 1303 cm^{-1}.

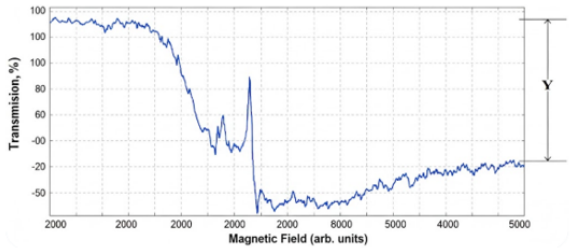

Figure 4: ESR spectrum of PS.7.1.S-0,01.

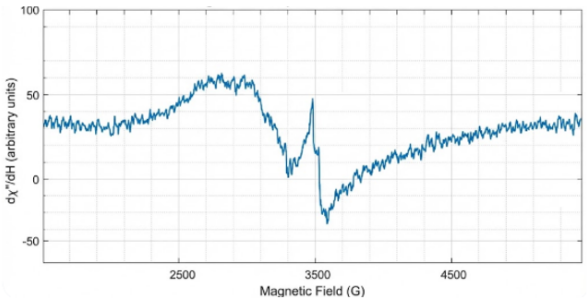

Figure 5: ESR spectrum of PS.7.1.S-0.90.

In order to form a well-grounded conviction that the broadening of the ESR line width observed in our experiments is not related to any inorganic elements, we first used X-ray fluorescence analysis to more thoroughly investigate the structure of the soot [16].

X-ray fluorescence analysis shows the presence of elements such as Kr, Nb, Ru, In, and Cs, with the quantitative content of all these elements combined not exceeding 0.1% of the total composition of the soot, which corresponds to the manufacturer's data on the filler [17]-[20].

To address the question of whether the studied object is an effectively isotropic system, it is necessary to conduct experiments on the angular dependence of the ESR signals. The results of our experiments on the angular dependence of the ESR signals are shown in Figures 6-7. As can be seen from the figures, when rotated at three different angles relative to the original position, the following are observed:

1) A clear variation in the intensity of the narrow doublet signal;
2) Practically no dependence of the intensity of the large overall signal on the angular rotations.

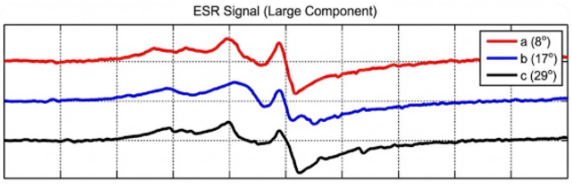

Figure 6: Angular dependence (a – 8°, b – 17°, c – 29°) of the large overall ESR signal of PS.7.1.S-0.09.

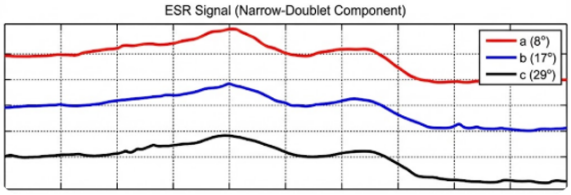

Figure 7: Angular dependence (a – 8°, b – 17°, c – 29°) of the narrow-doublet component of the ESR of PS.7.1.S-0.09.

Tables 1-2 show the concentration dependence of the main parameters of the large overall ESR signal and the narrow-doublet component in the composites. From this, it can be seen that each of these parameters can independently reflect the structural features of the object under study [21]-[26].

Table 1: Concentration dependence of the main parameters of the large overall ESR signal in the composites.

V_1	g	N, spin/g	T_1, sec	T_2, sec	$\left(\frac{hv}{hc}\right)$, cm^{-1}	H_{pp}, kA/m
0,01	2,083	$2,6 \cdot 10^{15}$	$1,03 \cdot 10^{-1}$	$6,5 \cdot 10^{-10}$	0,313	46,2
0,04	2,057	$1,6 \cdot 10^{15}$	$8 \cdot 10^{-2}$	$8,6 \cdot 10^{-10}$	0,33	35,0
0,09	2,128	$3,8 \cdot 10^{15}$	$7,5 \cdot 10^{-2}$	$6 \cdot 10^{-10}$	0,324	40,7
0,20	2,025	$1,5 \cdot 10^{15}$	$8 \cdot 10^{-2}$	$6,2 \cdot 10^{-10}$	0,331	41,3

Table 2: Concentration dependence of the main parameters of the ESR narrow-doublet component.

V1	ΔHpp, E	T1, sec	T2, sec	g	ΔW, eV	hA02, eV
0,01	21,0	8,8·10-4	5,6·10-9	2,034	4,1·10-5	5,44·10-7
0,04	21,5	4·10-4	3,99·10-9	2,029	4,08·10-5	4,6·10-7
0,09	22,0	1,1·10-3	6,2·10-9	2,032	4,08·10-5	3,7·10-7
0,20	18,3	1,6·10-4	4·10-9	2,031	4,08·10-5	3,3·10-7

In our studies on the frequency dependence of the conductivity of soot-filled polystyrene composites, both low and high frequencies of the alternating field were used. The dielectric characteristics and conductivity dependencies in the alternating field were recorded in the frequency range of 5×10^6 s^{-1}. The relative error in measuring the dielectric parameters on the instruments did not exceed 3%.

Figures 8-9 present the frequency dependence of the conductivity and dielectric losses of soot-filled PS.7.1.

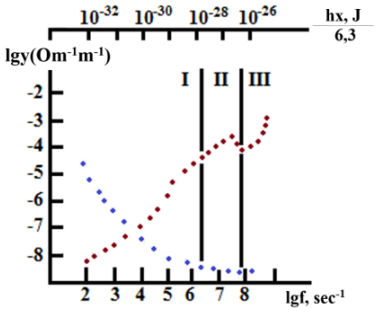

Figure 8: Frequency dependence of the conductivity of the composite.

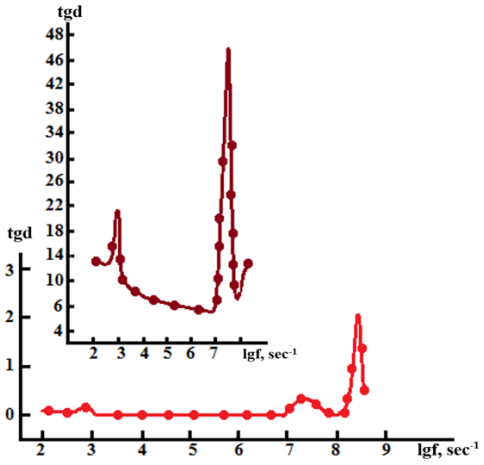

Figure 9: Frequency dependence of the dielectric losses of the composite.

3 CONCLUSIONS

Using the IR spectrum for PS.7.1, PVDF5.1, and the system PS.7.1.S, PVDF.5.1.S, chemical bonds involving C, H, and O in the interfacial layer of the composites were detected.

For the first time, stable paramagnetic centers (PMCs) were identified in soot-filled samples of PS.7.1 and PVDF.5.1, which allow for significant broadening of the ESR line and, based on these parameters, have the potential to compete with classical magnets.

Isotropic and anisotropic components of the ESR were identified in the composites PS.7.1.S and PVDF.5.1.S. The reason for the strong broadening of the ESR signals in the composites PS.7.1.S and PVDF.5.1.S is explained through an indirect mechanism of exchange interaction. For the first time, the configuration of PMCs in the composites PS.7.1.S and PVDF.5.1.S was demonstrated.

A lack of direct correlation between the main paramagnetic parameters of the composites PS.7.1.S and PVDF.5.1.S and the concentration of added soot was revealed, and for the first time, the light sensitivity of the compositions PS.7.1.S and PVDF.5.1.S was discovered.

REFERENCES

[1] A. I. Kuznetsov, V. N. Mochalin, and A. Yaroshenko, “Carbon-based nanocomposites: Structure, properties, and applications,” Carbon, vol. 167, pp. 1–27, 2020.

[2] D. I. Kamalova, A. V. Umarov, S. S. Negmatov, and N. S. Abed, “Electron–vibrational spectra of composites based on polystyrene and kaolin,” Composite Materials, no. 3, pp. 42–44, 2019.

[3] S. R. Dhakate and T. Yokozeki, “Polymer composites with carbon fillers: Electrical and magnetic properties,” Compos. Sci. Technol., vol. 195, pp. 108–118, 2020.

[4] L. Bokobza, “Multiwall carbon nanotube elastomeric composites: A review,” Polymer, vol. 48, no. 17, pp. 4907–4920, 2007.

[5] D. S. Su and J. Zhang, "Soot and carbon black in polymer composites," Prog. Polym. Sci., vol. 35, pp. 923–958, 2010.

[6] H. J. Butt, K. Graf, and M. Kappl, Physics and Chemistry of Interfaces. Weinheim, Germany: Wiley-VCH, 2013.

[7] M. N. R. Ashfold and A. J. Orr-Ewing, "Vibrational spectroscopy of polymers: Insights into molecular structure," J. Mol. Struct., vol. 1220, 2020.

[8] A. Grishin, "Electron paramagnetic resonance of carbonaceous materials," Appl. Magn. Reson., vol. 46, pp. 303–320, 2015.

[9] V. T. Lebedev, "Magnetic resonance in polymer composites," Polym. Sci. Ser. A, vol. 55, no. 6, pp. 393–405, 2013.

[10] J. K. Fink, Polymer Nanocomposites: Synthesis, Characterization, and Applications. Amsterdam, Netherlands: Elsevier, 2018.

[11] T. Enoki, M. Endo, and M. S. Dresselhaus, Carbon Nanostructures and Applications of Graphene and Carbon Nanotubes. Amsterdam, Netherlands: Elsevier, 2019.

[12] A. P. Roberts, "Interfacial chemistry in carbon–polymer systems," J. Appl. Polym. Sci., vol. 139, no. 16, 2022.

[13] C. Thomsen and S. Reich, "Raman and vibrational spectroscopy of carbon-based composites," Philos. Trans. R. Soc. A, vol. 362, pp. 2271–2288, 2004.

[14] Y. Wang and H. Hu, "Electrical and structural properties of soot–polymer composites," Adv. Compos. Hybrid Mater., vol. 5, pp. 651–664, 2022.

[15] L. J. Buckley, "EPR spectroscopy in polymer research," Macromolecules, vol. 35, no. 19, pp. 7355–7362, 2002.

[16] Z. Spitalsky, D. Tasis, K. Papagelis, and C. Galiotis, "Carbon nanotube–polymer composites: Chemistry, processing, mechanical and electrical properties," Prog. Polym. Sci., vol. 35, no. 3, pp. 357–401, 2010.

[17] A. Amari et al., "Enhanced photocatalytic water splitting for green hydrogen production and enrofloxacin degradation using a novel In_2S_3-based ternary photocatalyst: Fabrication and mechanism insights," Surf. Interfaces, vol. 58, Art. no. 105816, 2025.

[18] H. A. El-Sabban et al., "Visible light-driven photocatalytic degradation of norfloxacin by biochar-supported $Cs_3Bi_2I_9$–Bi_2MoO_6 Z-scheme composite: Characterization, optimization, and toxicity assessment," J. Water Process Eng., vol. 70, Art. no. 107131, 2025.

[19] M. S. Alshammari et al., "Novel environmentally benign dual Z-scheme $SrTiO_3$/g-C_3N_4/ZnO heterojunction for efficient H_2 evolution and polluted water treatment," FlatChem, vol. 50, Art. no. 100841, 2025.

[20] J. Huang et al., "Constructing a novel Z-scheme Fe_2O_3/$ZnIn_2S_4$@Bi_2WO_6 photocatalyst for boosting removal of non-biodegradable ciprofloxacin and long-term stable CO_2 conversion," J. Water Process Eng., vol. 72, Art. no. 107632, 2025.

[21] S. S. Nasriddinov and D. M. Esbergenov, "A study of complex defect formation in silicon doped with nickel," Russ. Phys. J., vol. 65, no. 9, pp. 1559–1563, 2023.

[22] S. S. Nasriddinov, "Investigation of temperature sensors based on Si⟨P,Ni⟩," J. Nano- Electron. Phys., vol. 7, no. 3, Art. no. 03037, 2015.

[23] A. S. Rysbaev et al., "On new two-dimensional structures produced on the Si (111) and Si (100) surface upon molecular-beam epitaxy of cobalt and silicon," J. Surf. Investig., vol. 5, no. 6, pp. 1193–1196, 2011.

[24] M. K. Bakhadyrkhanov et al., "Features of thermal properties of strongly compensated Si⟨B,Mn⟩," Inorg. Mater., vol. 45, no. 11, pp. 1210–1212, 2009.

[25] M. K. Bakhadyrkhanov et al., "Impurity photovoltaic effect in silicon with multicharge Mn clusters," Appl. Sol. Energy, vol. 44, no. 2, pp. 132–134, 2008.

[26] M. T. Normuradov et al., "Variations in the electronic structure of the silicon near-surface region during implantation of phosphorus and boron ions," J. Commun. Technol. Electron., vol. 52, no. 8, pp. 898–900, 2007.